RESEARCH ARTICLE

Check for updates

Sponge-like macroporous cyclodextrin-based cryogels for controlled drug delivery†

Chiara Zagni, [iD] ‡[a] Alessandro Coco, [iD] ‡[b] Tommaso Mecca,*[c] Giusy Curcuruto,[b] Vincenzo Patamia, [iD] [a] Katia Mangano,[d] Antonio Rescifina [iD] *[ab] and Sabrina Carola Carroccio [iD] [b]

New drug delivery systems for wound healing applications based on α/β/γ-cyclodextrin (α/β/γ-CD) acrylic (A) and styrenic (S) monomers have been synthesized and co-polymerized with 2-hydroxyethyl methacrylate (HEMA) *via* a cryo-polymerization technique. The 3D macroporous cryogels containing hydrophobic cavities were loaded with lomefloxacin (LOM), piroxicam (PIR), and fluconazole (FLU) with a drug loading efficiency (DLE) of up to 78%. Depending on the formulated systems, the release of drugs under different stimuli was achieved, with efficiencies ranging from 23 to 95%. It was demonstrated that the presence of CDs within cryogels determines benefits both in loading capacity and drug delivery. CD derivatives were simultaneously loaded with LOM and PIR and tested for multi-drug release. This non-conventional approach was successfully designed as a proof of concept responding to the need to preserve a sterile target area, facilitating skin repair in wound healing applications. For this purpose, the biocompatibility of CD formulations was ascertained against human fibroblasts.

Introduction

Delivery systems' design is of great interest in the pharmaceutical field.[1] Based on both their bio and synthetic nature, macromolecular architectures are widely studied as drug carriers to achieve controlled release and targeted drug delivery while reducing the side effects.[2] Targeting a body area, such as an organ or cellular and subcellular levels of specific tissues, allows for overcoming the toxic effects of conventional drug delivery, thereby reducing the amount of drug required for therapeutic efficacy.[3]

Among the carriers, liposomes have been extensively used thanks to their safety and ability to incorporate hydrophilic and hydrophobic drugs.[4] However, their physical and chemical instability can lead to (i) side effects, (ii) efficacy reduction, and finally, (iii) lack of the ability to achieve a controlled release of the drugs.[5]

Natural polymeric micelles are novel drug carriers with numerous advantages, such as selective targeting, reduced side effects of drugs, and stable storage.[6] Overall, polymeric matrices derived using a synthetic procedure can be chemically modified and shaped to host pharmaceuticals, improving their practical therapeutic efficacy and mitigating their side effects.[7]

Often in the drug delivery field, a common limitation is the effective delivery of hydrophobic drugs. In this context, cyclodextrins (CDs), thanks to their unique structure that can accept hydrophobic guests in hydrophilic solvents, are often employed in polymeric systems.[8] Indeed, CDs inserted in polymeric structures have been successfully used as auxiliaries to solubilize poorly soluble drugs.[9] The polymeric formulation is responsible for the drug release rate, loading capacity, bioavailability, and biocompatibility. In the case of wound dressing, the polymeric system has to maintain sterility in the target area and assist in facilitating the repair.

Formulating drug-loading materials for repairing skin wounds such as burns, surgical wounds, decubitus ulcers, *etc.* is still a challenge. An ideal material for wound dressing should have certain features such as (1) non-cytotoxicity, (2) high oxygen permeability, (3) ease of removal from the wound, and (4) the ability to maintain the relative humidity since a wet microenvironment of the wound bed is suitable for cell migration and cytokine secretion, which promotes wound healing.

Hydrogels, which possess the features mentioned above, have been extensively used in the last few years for wound dressing. However, they also present some drawbacks, such as poor

[a] Department of Drug and Health Sciences, University of Catania, V.le A. Doria 6, 95125, Catania, Italy. E-mail: arescifina@unict.it
[b] Institute for Polymers, Composites, and Biomaterials CNR-IPCB, Via Paolo Gaifami 18, 95126, Catania, Italy
[c] Institute of Biomolecular Chemistry CNR-ICB, Via Paolo Gaifami 18, 95126, Catania, Italy. E-mail: Tommaso.mecca@icb.cnr.it
[d] Department of Biomedical and Biotechnological Sciences, Oncologic, Clinical, and General Pathology Section, University of Catania, Catania, Italy
† Electronic supplementary information (ESI) available: NMR, MALDI-TOF MS, and FT-IR spectra; TGA, calibration curves, *in vitro* release profiles; and kinetics release parameters. See DOI: https://doi.org/10.1039/d3qm00139c
‡ These authors contributed equally.

mechanical properties[10] and oxygen permeation.[11] These issues may be overcome by using cryogels as a wound-healing patch.

Cryogels continue to receive considerable scientific and industrial attention for their prominent features, such as super-absorbent properties, high loading capacities, the ability to modulate drug release profiles, and biocompatibility.[12] They find application in tissue scaffolding, drug delivery, cell transplantation, and stem-cell-based therapies because of their excellent biocompatibility features.[13–15]

As an additional advantage, the synthetic process based on a radical polymerization process occurring in a frozen state is effective, cost-saving, and sustainable because the solvent used to produce them is water.[16] This peculiar procedure, which is mostly applicable to water-soluble monomers, generates interconnected macroporous cryogels, the dimensions of which can be tuned by changing the polymerization parameters.[17] The distinctive morphology of cryogels improves their elasticity and mechanical properties compared to hydrogels.[18]

Compared to parent hydrogels, they exhibit significantly improved drug protection[19] and excellent oxygen permeability,[20] as well as a high drug-loading ability and better absorption capacity.[21] Interestingly, depending on the application, their oxygen permeability may be modulated as a function of the dimension of the pores.[22]

Among the monomers, we selected HEMA because it produces a hydrophilic and biocompatible cryo-polymer with high water uptake that ensures the exudates' absorption without losing the appropriate level of moisture.[23,24]

Nevertheless, hydrophilicity determines the lack of adsorption of hydrophobic species. Specifically, hydrophobic drugs are generally incompatible with hydrogels.[25] A strategy to overcome this problem is to design host–guest supramolecular systems with hydrophobic cavities, such as self-assembling peptide nanostructures,[26] cucurbit[n]uril-based functionalized microcapsules,[27] calix[4]arenes,[28] dendrimers, hyperbranched or star polymers,[29] and polymeric nanocarriers based on cyclodextrins.[30]

Thanks to their unique peculiarities, CDs are among the most used supramolecular drug delivery systems. They are cheap, biocompatible, and biodegradable macrocyclic oligosaccharides composed of α-(1,4)-linked glucopyranose subunits. Specifically, the three cyclodextrins α-CD, β-CD, and γ-CD consist of six, seven, and eight glucopyranose units forming a cage-like supramolecular structure that can encapsulate different active hydrophobic ingredients.[31] The versatile design and tunable features of CD-polymers (poly-CDs) combine the polymers' advantages with CD's ability to form inclusion complexes.[32] Poly-CDs can increase the ability to encapsulate guest molecules, improve drug stability, and efficiently regulate the drug release rate.[33]

This work introduces a novel approach that takes advantage of the versatility of radical polymerization of new CD monomers by utilizing a cryo-polymerization process, obtaining hydrophilic sponge-like materials that are effective in loading hydrophobic drugs.

Specifically, macroporous interconnected 3D hydrophilic structures were synthesized based on HEMA and $\alpha/\beta/\gamma$-CD functionalized with acrylic (A) and styrenic (S) monomers. The as-prepared acrylic (Acr) and styrenic (Styr) cryogel samples, named Acr-α-CD, Acr-β-CD, Acr-γ-CD, Styr-α-CD, Styr-β-CD, and Styr-γ-CD, were loaded with antibiotic (lomefloxacin, LOM), anti-inflammatory (piroxicam, PIR), and antifungal (fluconazole, FLU) drugs and their release as a function of cavity dimensions was tested in acidic and saline solutions. Also, a multi-drug system was prepared by loading anti-inflammatory and antibiotic drugs into the same cryogel for simultaneous release and was tested as a potential administration method for pharmaceuticals using a smart patch for wound healing applications.

In biomedical applications, bacterial cellulose and chitosan-based polymers, not including pharmaceuticals, have already been reported for wound dressing to maintain a sterile environment.[34,35] Besides this, poly(vinyl alcohol) cryogel membranes comprising resveratrol have also been produced for skin application. However, as reported by the authors, the lack of a macroporous network and the dense consistency obtained in the presence of resveratrol induced low water uptake capacity.[36] Among the limited literature regarding delivery systems of PIR, Farooq et al. reported the preparation of biodegradable electrospun nanofibrous mats and cast films from poly(vinyl alcohol), chitosan, and hydroxyapatite for insertion into periodontal pockets.[37]

Herein, we propose a unique drug delivery system (DDS) for patch uses, which is able to release piroxicam and other drugs, such as an antibiotic (lomefloxacin) and an antifungal (fluconazole) drug in skin wound healing. To our knowledge, cryogels for patch applications in wound healing that can load multi-drugs and release them under specific conditions have not been reported.

Experimental section

Materials

α-CD, β-CD, γ-CD, acryloyl chloride, 4-vinyl-benzyl chloride 90%, sodium hydride in mineral oil (69%), acetone, dimethyl-formamide anhydrous (DMF), 2-hydroxyethyl methacrylate (HEMA), N,N'-methylene-bisacrylamide (MBAA), ammonium persulfate (APS), tetramethyl-ethylene-diamine (TEMED), ethanol (99.9%), sodium hydride 60% in mineral oil, hydrochloric acid (37%), DMSO (99.7%), and trifluoroacetic acid (TFA) were purchased from Merk. LOM, FLU, and PIR were obtained (assigned purity >99%) from Medivis srl. A Milli-Q water purification system was used to produce deionized water.

Synthesis

Synthesis of α-CD-acrylate monomer (A-α-CD) 1. α-CD (0.5 g, 0.5139 mmol) was dissolved in DMF (7 mL) in a round-bottom flask under a nitrogen environment and NaH (82.3 mg, 2.0558 mmol, 4 eq.) was added at 0 $^\circ$C and the reaction mixture was stirred for 1 h. After that, acryloyl chloride (171 μL, 2.0558 mmol, 4 eq.) was added dropwise. The reaction was carried out for 24 h at r.t. with stirring. Then, it was poured into a rotavapor to concentrate the solution.[38] Cold acetone was added, and the solid was recovered by filtration and dried for

24 h in a drying oven. Yield = 85%. ^{1}H NMR (500 MHz, DMSO-d$_6$): δ = 6.43–6.03 (m, 4H), 5.99–5.76 (m, 2H), 5.72–5.34 (m, 12H), 4.88–4.70 (m, 6H), 4.66–4.33 (m, 8H), 3.85–3.71 (m, 7H), 3.69–3.56 (m, 16H), 3.31–3.24 (m, 6H); ^{13}C NMR (126 MHz, DMSO-d$_6$): δ = 165.67, 130.62, 101.87, 82.09, 73.28, 72.12, 60.03, 35.82, 33.93, 30.80.

Synthesis of α-CD-styrenate monomer (S-α-CD) 2. The title compound (pale yellow powder) was prepared analogously to compound **1**. α-CD (0.5 g, 0.5139 mmol), NaH (82.3 mg, 2.0558 mmol, 4 eq.), 4-vinyl benzyl chloride (313.7 μL, 2.0558 mmol, 4 eq.). Yield = 74%. ^{1}H NMR (500 MHz, DMSO-d$_6$): δ = 7.67–7.53 (m, 4H), 6.88–6.74 (m, 2H), 5.96 (d, J = 12.0 Hz, 2H), 5.38 (d, J = 12.0 Hz, 2H), 4.84–4.72 (m, 6H), 3.84–3.72 (m, 6H), 3.69–3.55 (m, 18H), 3.44–3.19 (m, 24H); ^{13}C NMR (126 MHz, DMSO-d$_6$): δ = 138.85, 135.85, 133.43, 127.42, 126.51, 116.17, 101.91, 82.11, 73.27, 72.11, 66.74, 60.02, 48.10.

Synthesis of β-CD-acrylate monomer (A-β-CD) 3. The title compound (white powder) was prepared analogously to compound **1**. β-CD (0.5 g, 0.5139 mmol), NaH (70.5 mg, 1.7621 mmol, 4 eq.), acryloyl chloride (146.5 μL, 1.7621 mmol, 4 eq.). Yield = 83%. ^{1}H NMR (500 MHz, DMSO-d$_6$): δ = 6.42–6.29 (m, 3H), 6.26–6.14 (m, 3H), 5.94–5.84 (m, 3H), 5.81–5.57 (m, 13H), 4.90–4.76 (m, 7H), 4.55–4.39 (m, 10H), 3.72–3.45 (m, 32H); ^{13}C NMR (126 MHz, DMSO-d$_6$): δ = 101.89, 81.50, 73.06, 72.43, 72.02, 59.90, 35.79.

Synthesis of β-CD-styrenate monomer (S-β-CD) 4. The title compound (pale yellow powder) was prepared analogously to compound **1**. β-CD (0.5 g, 0.4405 mmol), NaH (70.5 mg, 1.7621 mmol, 4 eq.), 4-vinyl benzyl chloride (275.9 μL, 1.7621 mmol, 4 eq.). Yield = 71%. ^{1}H NMR (500 MHz, DMSO-d$_6$): δ = 7.59 (q, J = 8.2 Hz, 3H), 7.51–7.25 (m, 9H), 6.85–6.66 (m, 3H), 6.02–5.87 (m, 2H), 5.88–5.74 (m, 4H), 5.39–5.36 (m, 1H), 5.30–5.14 (m, 3H), 4.87–4.74 (m, 7H), 3.70–3.47 (m, 32H); ^{13}C NMR (126 MHz, DMSO-d$_6$): δ = 138.83, 136.37, 135.86, 133.54, 128.46, 127.48, 125.99, 116.18, 114.34, 102.01, 81.51, 73.17, 73.03, 72.46, 66.65, 59.93.

Synthesis of γ-CD-acrylate monomer (A-γ-CD) 5. The title compound (white powder) was prepared analogously to compound **1**. γ-CD (0.5 g, 0.3855 mmol), NaH (61.67 mg, 1.5419 mmol, 4 eq.), acryloyl chloride (128.6 μL, 1.5419 mmol, 4 eq.). Yield = 86%. ^{1}H NMR (500 MHz, DMSO-d$_6$): δ = 6.43–5.98 (m, 7H), 5.82–5.64 (m, 12H), 4.97–4.82 (m, 8H), 4.62–4.47 (m, 9H), 3.73–3.49 (m, 32H), 3.40–3.34 (m, 6H); ^{13}C NMR (126 MHz, DMSO-d$_6$): δ = 130.63, 101.62, 80.87, 72.93, 72.14, 59.96, 35.81, 33.96, 30.80.

Synthesis of γ-CD-styrenate monomer (S-γ-CD) 6. The title compound (yellow powder) was prepared analogously to compound **1**. γ-CD (0.5 g, 0.3855 mmol), NaH (61.67 mg, 1.5419 mmol, 4 eq.), 4-vinyl benzyl chloride (241.43 μL, 1.5419 mmol, 4 eq.). Yield = 75%. ^{1}H NMR (500 MHz, DMSO-d$_6$): δ = 7.66–7.54 (m, 5H), 7.49–7.35 (m, 6H), 6.88–6.66 (m, 4H), 6.01–5.89 (m, 2H), 5.42–5.33 (m, 2H), 5.31–5.20 (m, 2H), 4.93–4.81 (m, 8H), 3.73–3.56 (m, 38H); ^{13}C NMR (126 MHz, DMSO-d$_6$): δ = 162.28, 138.86, 136.37, 135.84, 133.42, 128.24, 127.39, 126.51, 125.99, 116.19, 101.70, 80.96, 80.92, 73.09, 72.14, 66.80, 60.01, 35.77, 30.63.

Synthesis of CD-HEMA cryogels. Acr/Styr-α/β/γ-CD cryogels were synthesized by a radical polymerization process. In detail, functionalized monomers of α/β/γ-CD and HEMA as co-monomers were dissolved in water at a molar ratio of 1:28.

The cross-linking agent N,N'-methylene bisacrylamide (MBAA) was added at a monomers/crosslinker molar ratio of 6:1 and mixed until complete dissolution. The amount of water was then corrected to obtain a total content of polymerizable compounds of 10% w/v of the solution. The mixture was cooled at 0 °C and then 1% v/v of a water solution of APS at a concentration of 10% w/v was added, followed by 1% v/v of a water solution of TEMED at a concentration of 10% w/v. The mixture was stirred for 1 minute, then distributed into 3 mL capped syringes (1 cm in diameter, ≈1 mL final volume) and poured into a cryostatic bath at −15 °C for 24 h. Afterward, the frozen samples were thawed, washed with water and ethanol, and dried under nitrogen flux; then, all samples were dried under a vacuum overnight at 40 °C.

Synthesis of HEMA cryogel. HEMA cryogel was synthesized, washed, and dried using the same procedure used to synthesize CD-HEMA cryogels.[39] All the subsequent operations were identical to the process used to synthesize CD-HEMA cryogels.

Characterization

NMR spectroscopy. ^{1}H and ^{13}C NMR spectra were recorded, at 300 K, on a Varian UNITY Inova spectrometer, at 500 MHz for ^{1}H NMR and 125 MHz for ^{13}C NMR. Chemical shift (δ) values are given in ppm.

Matrix-assisted laser desorption/ionization-time of flight mass spectrometry (MALDI-TOF MS) analysis

MALDI mass spectra (Fig. S1–S12, ESI†) were acquired in a reflector mode using a 4800 MALDI-TOF/TOF™ analyzer (Applied Biosystem, Framingham, MA, USA), equipped with an Nd:YAG laser (wavelength of 355 nm) and working in a positive-ion mode. The laser had a wavelength of <500 ps pulse and a 200 Hz repetition rate. The mass resolution of MALDI spectra was about 10 000 (full width at half maximum, FWHM) and mass accuracy was 1–10 ppm for masses in the range m/z 200–1000 Da. An appropriate amount of monomers 1–6 was dissolved in H$_2$O and mixed with the solution of 2,5-dihydroxybenzoic acid (DHB) matrix to obtain a 1:1 ratio. 1 μL of each sample/matrix mixture was spotted onto the MALDI sample holder and dried at 25 °C to allow matrix crystallization.

Fourier transform infrared (FTIR) analyses

FTIR analyses in the 4000–400 cm^{-1} region were performed using an FTIR System 2000 (PerkinElmer, Waltham, MA, USA) and KBr as medium.

Thermogravimetric analyses (TGA)

Thermal behaviors and kinetics parameters of the synthesized monomers and cryogels were determined using TA instruments operating software (New Castle, Delaware, US). The measurements were performed in a temperature range of 40 °C to 800 °C, at a heating rate of 10 °C min^{-1} under nitrogen flow (60 mL min^{-1}), using 5 ± 0.1 mg of sample.

Scanning electron microscopy (SEM)

Surface morphologies of cryogel samples were observed using a desktop scanning electric microscopy Thermo Phenom Prox system (Thermo Fisher Scientific – Waltham, MA, USA) (SEM)

combined with a fully integrated energy-dispersive X-ray detector (silicon drift detector). The samples were lyophilized before and after drug loading. ImageJ® software (National Institutes of Health, Bethesda, MD, USA) was used to measure the pore size. Energy-dispersive X-ray spectroscopy (EDX) was used to determine the chemical composition of all the prepared materials.

Swelling test

Before the measurements of swelling properties, each cryogel was cut into small specimens of 9 mm diameter and 10 mm length. The samples were placed in excess deionized water to enable complete washing out of the unreacted monomer, initiator, or soluble polymer. Water was replaced twice daily until the samples reached a swelling equilibrium at room temperature. Before weighing, each sample was taken out from the water, and surface water was blotted. Each sample was weighed at least three times to perform accurate measurements. Afterward, the swollen samples were dried in a freeze-dryer and again weighed. For each type of cryogel, all measurements were repeated with three parallel samples, and the average result was calculated. The standard deviation was less than 5%.

Drug loading

First, PIR and FLU were dissolved in a mixture of DMSO/H_2O 2 : 1 at a concentration of 1 mg mL^{-1}, while LOM was dissolved in H_2O at the same final concentration of 1 mg mL^{-1}. Then, 250 μL of each solution was loaded into 10 mg of dried cryogel separately. For the multi-drug loading experiment, 250 μL of PIR 1 mg mL^{-1} was mixed with 250 μL of LOM 1 mg mL^{-1}, and a final volume of 500 μL of the prepared solution was added to 10 mg of dried cryogel. The samples were incubated for 24 h in the dark. The solvent was removed by multiple washes with a total volume of 3 mL of water. Aqueous wastes were collected to measure the discarded amount of the drug using a UV-vis spectrophotometer, allowing the estimation of the actual loading capacities. Subsequently, the drug-loaded cryogels were frozen and freeze-dried for 24 h. The tests were performed in triplicate.

Drug loading efficiency (DLE) or drug loading content was calculated from the following equation:[40]

$$\text{DLE (\%)} = \frac{\text{Weight of loaded drug}}{\text{Weight of total drug}} \times 100$$

Drug release

Each drug-loaded freeze-dried cryogel was tested for drug release in an acidic solution and saline buffer at 37 °C. The acidic solution was prepared by adding HCl to water up to a pH of 3, while the saline buffer consisted of a ready solution of PBS (phosphate-buffered saline, pH 7.4).

Each sample was placed in a vial with 10 mL of solution (acidic and saline), and different aliquots were collected at different times: 10 and 30 minutes, 1, 2, 3, 4, 5, 8, and 24 hours. The released amount of drug was determined using a UV-vis JASCO spectrophotometer.

The cumulative amount of drug released was calculated using a UV-vis JASCO spectrophotometer based on the calibration curves in the specific medium (Fig. S21 and S22, ESI†), in a concentration range of 0.010–0.025 mg mL^{-1} for LOM, PIR, and FLU, and a concentration range of 0.005–0.020 mg mL^{-1} for the multi-drug solution.

After each measurement, the collected aliquots were reinserted into the vial with the samples not to change the release volume and maintain a cumulative concentration of the drug released. The tests were performed in triplicate.

Drug release efficiency (DRE) was calculated from the following equation:

$$\text{DRE (\%)} = \frac{\text{Mass released drug}}{\text{Mass loaded drug}} \times 100$$

Kinetics of release. The release behavior of all CD-HEMA cryogels and HEMA cryogels, used as a control with various drugs, has been compared with mathematical models primarily used in drug delivery.[41] Data points within the first 3 hours of release were used for the fitting process to avoid interference from the saturation of the medium with the real system kinetics.

Equations chosen:

Zero-order kinetics:

$$M_t/M_\infty = k_0 t$$

This kinetic equation expresses a constant release over time, often related to solid dissolution.[42]

First-order kinetics:

$$M_t/M_\infty = 1 - e^{-k_1 t}$$

In this case, the drug release is concentration-dependent; thus, it decreases with time.[43]

Korsmeyer–Peppas model:

$$M_t/M_\infty = k_3 t^n$$

This equation has been designed to describe drug release from polymeric matrix systems as hydrogels.[44] The model is useful when the release mechanism is unclear or when different factors influence it. Depending on the n value, it is possible to distinguish Fickian diffusion, anomalous transport, case I transport, and super case II transport.[45]

Higuchi model:

$$M_t/M_\infty = k_2 t^{\frac{1}{2}}$$

This represents one of the most used models for drug release from matrix systems, mainly thin films or membranes. The relation considers particle diffusion through homogeneous matrices.[46]

Weibull model:

$$M_t/M_\infty = 1 - \exp(-at^b)$$

This model is mainly used to compare matrix systems and their drug-release kinetics.

In all the mentioned equations, M_t represents the cumulative release at time t; M_∞ is the amount of drug loaded in the system at time 0; t is the release time; while the various k values are the kinetic constants, and other factors such as n, a, and b are specific indices.[47]

Biocompatibility cellular test. Human dermal fibroblasts (HDF; 106-05a), 5000 cells per well (obtained from ECACC, Sigma) were used to determine the cytocompatibility of the synthesized cryogels. Cells were cultured on 96-well plates for 24 h in DMEM with 10% v/v FBS and $1\times$ v/v penicillin-streptomycin at 37 °C in a 5% CO_2 incubator. The cryogel samples (5 mg) were added to cells, at 80% confluence, for 72 h. MTT [3-(4,5-dimethylthiazol-2-yl)-2,5-diphenyltetrazolium bromide] assay was used to assess the cell viability. The optical density of the dissolved formazan crystals was quantified at 575 nm using spectrophotometric analysis (Tecan Sunrise Microplate Reader).

Results and discussion

Synthesis and characterization of monomers and cryogels

An appropriate macromolecular container design is crucial to maximize drug benefits and avoid adverse collateral reactions. In light of this, using cryogels could be an effective and valuable strategy in this field. To perform the cryo-polymerization reaction of $\alpha/\beta/\gamma$-cyclodextrin ($\alpha/\beta/\gamma$-CD) derivatives, a preliminary functionalization of monomers was accomplished. Nucleophilic substitution of $\alpha/\beta/\gamma$-cyclodextrins with acryloyl chloride and 4-vinyl-benzyl chloride to form the corresponding acrylic and styrenic monomers was performed using a molar ratio of CD/acryloyl or 4-vinyl-benzyl chloride of 1:4 (Scheme 1). Despite the

presence of many hydroxyl groups in the skeleton of cyclodextrins, each –OH possesses a distinct reactivity; in fact, primary hydroxyls at the C6 position are the most basic and nucleophilic and, consequently, the most reactive.[48] NMR spectroscopic analysis and MALDI experiments were used to determine the degree of cyclodextrin substitution. The number of substituents introduced on the cyclodextrin was strictly correlated to the dimension of CD. It has been observed that a more extensive substrate cavity corresponds to an increase in the degree of substitution when the added moiety is bulky, like the 4-vinyl-benzyl group. Therefore, β and γ-CD monomers resulted in tri-, tetra-, and even penta-4-vinyl-benzyl substitution, while α-CD was only mono- or di-substituted.

Regarding the acrylic group, the behavior of all three cyclodextrins was similar, with a degree of substitution of 3. Spectral analysis also showed that the bulkiest 4-vinyl-benzylic moiety binds less effectively to the CD than the acrylic one, which determines lower yields. The ^{1}H-NMR spectra (Fig. S1–S12, ESI†) showed that after the reaction of α, β, and γ-CDs with acryloyl chloride and 4-vinyl-benzyl chloride, characteristic olefinic proton signals appeared in a range from 5.74 to 6.33 ppm, indicating the presence of unsaturated double bonds. The degree of substitution was calculated by comparing the integral of the protons at the terminal carbon of D-(+)-glucopyranose of CD, the peak at position 2. The success of the reaction of α, β, and γ-CDs with 4-vinyl-benzyl chloride was confirmed by the presence of benzylic hydrogens in the range of 7.23–7.74 ppm.
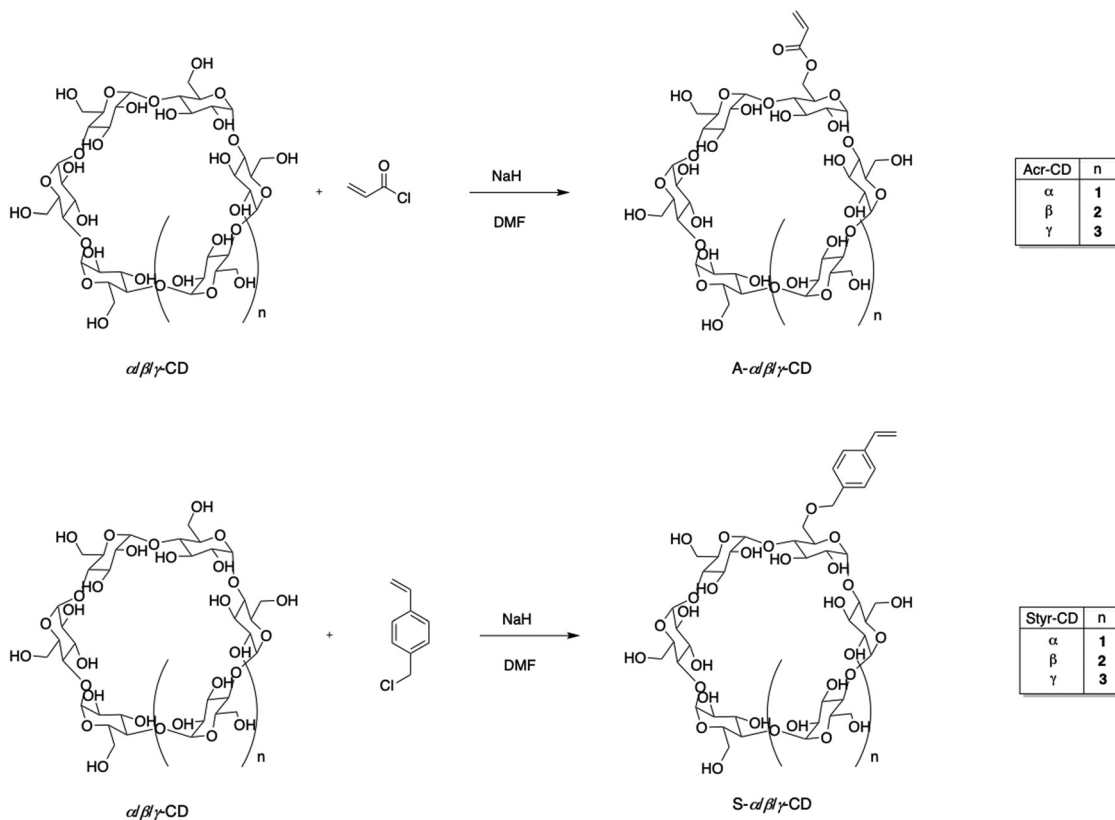
Scheme 1 Synthesis of acryloyl $\alpha/\beta/\gamma$-CDs and 4-vinyl-benzyl $\alpha/\beta/\gamma$-CD monomers.

According to MALDI analysis (Fig. S13–S18, ESI†), the obtained cyclodextrin monomers have a different degree of substitution based on the dimension of their cavity and reagents used.

Considering the steric hindrance of the CD substrate, which could negatively influence the polymerization process, a co-monomer was used to synthesize the final cryogels (Scheme 2). Specifically, HEMA was selected by carrying out two reactions with different CD/HEMA molar ratios (1 : 10 and 1 : 28). It was found that the CD/HEMA ratio influenced the yield of polymerization, which was assessed to be 80% in the case of the 1 : 28 CD/HEMA molar ratio compared to 50% for the 1 : 10 ratio, while the HEMA cryogel was synthesized with a yield of 85%.

The chemical structure of the synthesized copolymers was confirmed by FTIR analysis. The infrared spectra of cryogels Acr-α-CD, Acr-β-CD, Acr-γ-CD, Styr-α-CD, Styr-β-CD, and Styr-γ-CD are shown in Fig. S19 (ESI†) and show the disappearance of the pattern of the typical signal related to methylene (–C=C) groups of the monomers in the range 1000–800 cm^{-1}, confirming the formation of a polymeric sponge. The spectra present characteristic diagnostic bands at 3400–3100, 3000–2780, 1650, and 1082 cm^{-1} related to the stretching vibrations of the O–H, C–H, C=O, and C–O groups, respectively. Additionally, a broad transmittance peak at 3292 cm^{-1} is due to the valence vibrations of O–H bonds (C–OH).

The thermal stability of CD-HEMA cryogels was investigated using TGA (Fig. S20, ESI†). The weight loss was recorded up to 800 °C, calculating temperatures at 5% of weight loss (T_5, °C), temperatures at the maximum rate of degradation (T_{max}, °C),

and residual masses (wt%). As shown in Table 1, all samples are characterized by an initial weight loss in the 80–140 °C range, most likely due to the dehydration of CDs and cryogels.[49,50] Thermal degradation of HEMA-CD cryogels started from 270 to 480 °C, including the (i) degradation of cyclodextrins to form CO_2, levoglucosan, and furan compound and, (ii) unzipping HEMA reactions to form HEMA monomers. Specifically, the residues obtained at 800 °C for acrylate cryogels are derived from cyclodextrins that tend to form char under inert conditions.[51] These findings further confirmed the success of the polymerization of the cyclodextrin-based monomers. In the case of styrene derivatives, residues can also arise from the presence of styrene groups that typically produce char-like structures (Mecca CEJ 2020).

To determine the swelling properties, the standard gravimetric procedure was used as described.[52] As expected, all materials showed a swelling ratio inferior to that of HEMA used as the control (Fig. 1a). Indeed, this finding can reasonably be ascribed to the high numbers of cross-linking moieties in the functionalized CD that affected absorption properties. Nevertheless, the increase in cross-linked bridges imparts excellent resistance to the cryogels during the loading/releasing tests.

Morphological analyses of the synthesized cryogels are shown in Fig. 1b–g. As observed from the micrographs, all materials showed peculiar open-cell morphology with an interconnected macroporous structure and the pore diameter ranging from 10 to 70 μm. This peculiarity is characteristic of the cryopolymerization process using monomers and cross-linkers at appropriate concentrations.

Drug loading

Polymeric gels based on cyclodextrins are gaining interest as vehicles for therapeutic agents, as they can incorporate drugs, ensuring a controlled release of the active ingredient.[53]

The capacity of the newly synthesized CD-HEMA cryogels to incorporate molecules within their structure was tested using LOM, PIR, and FLU as drug references. Fig. 2 shows all samples' drug loading efficiency (DLE). All the tested drugs were effectively incorporated into all the cryogels, where the presence of cyclodextrins made the difference. Indeed, drug loading efficiency differs among the cryogels depending on their network architecture.

For wound healing applications, the ability to release both anti-inflammatory and antibiotic drugs simultaneously surely
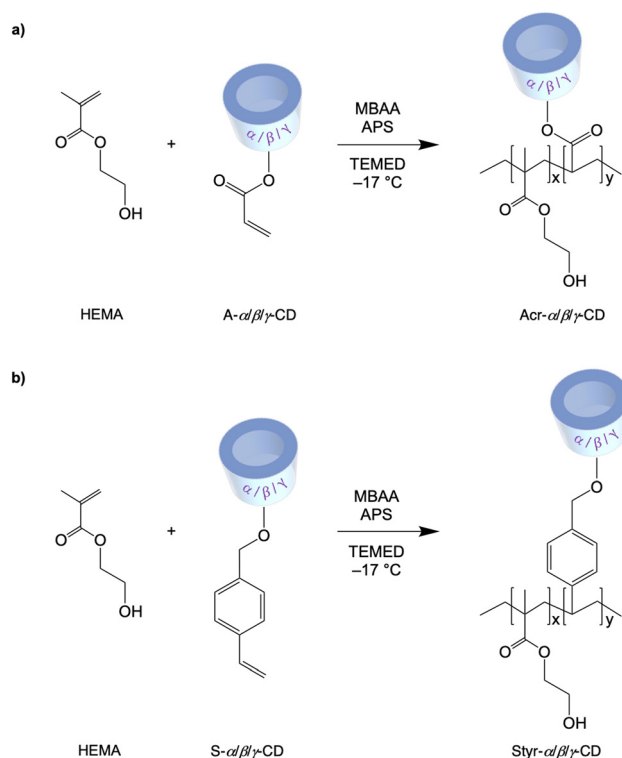
Scheme 2 Synthesis of Acr-α-CD, Acr-β-CD, Acr-γ-CD, Styr-α-CD, Styr-β-CD, and Styr-γ-CD cryogels.

Table 1 Temperatures at 5% weight loss, temperatures at a maximum decomposition rate, and residual masses at 800 °C of the synthesized cryogels

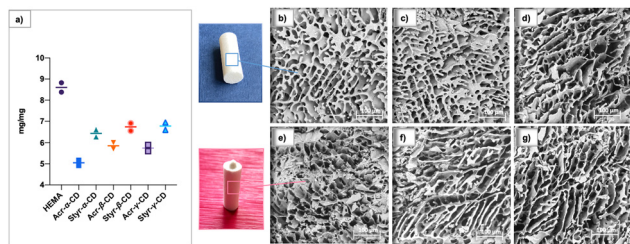| Sample	T_5 (°C)	T_{max} (°C)	Weight residue (wt%)
Acr-α-CD	122.23	427.97	2.38
Acr-β-CD	121.54	436.74	1.14
Acr-γ-CD	157.18	438.02	2.58
Styr-α-CD	95.21	440.17	3.48
Styr-β-CD	95.12	434.52	3.71
Styr-γ-CD	79.40	436.73	2.28

Fig. 1 (left) a) Swelling ratio of HEMA-CD cryogels. (right) SEM micrographs of the synthesized cryogels: (b) Acr-α-CD; (c) Acr-β-CD; (d) Acr-γ-CD; (e) Styr-α-CD; (f) Styr-β-CD; and (g) Styr-γ-CD. Scale bars are 100 μm.

could be an added advantage. In this view, we prepared and tested a multiloading system based on PIR and LOM, evaluating the DLE as a function of cryogel structures (Fig. 2d).

As well stated, drug loading depends on (i) the surface area, (ii) the solution uptake capacity related to the swelling ability of the system, (iii) the porous network, and (iv) the CD cavity dimensions. Generally, the larger and more flexible hydrophobic core better accommodates drugs, although selectivity may be compromised.[54]

It is worth noticing that not only CD functionalization contributes to the drug loading capacity, but also acrylic and styrenic moieties can help establish secondary interactions (H-bond and π–π staking) with used drugs contributing to the loading capacity.

As highlighted in Fig. 2a, the LOM loading capacity for the HEMA cryogel was 28% drug in the starting solution,

corresponding to 7 mg g^{-1}, whereas CD-HEMA cryogels have a drug loading capacity ranging from 8.8 to 17 mg g^{-1}. It is possible to assume that when the drug molecules are inside the cyclodextrin cavities, they can form H bonds between their –OH or –NH groups and the carbonyl groups of the CD acrylate moieties. Probably, when the acrylates are substituted with the styrenyl portion linked to the CDs by the oxygen, these bonds become weak or may be sterically hindered.

In particular, our experiments highlight how LOM uptake increases as the volume of the CD increases, while other studies have found that β-CD is best suitable for LOM, emphasizing the importance of the volume of the cavities.[55] In this case, the higher number of styrenic substituents in Styr-γ-CD could play a key role in LOM absorption forming π–π interactions.

PIR displayed a DLE of 46% of the drug solution prepared, which corresponds to 11.5 mg g^{-1} over HEMA and ranges from 44 to 64%, which means 11–16 mg g^{-1} for CD-HEMA cryogels (Fig. 2b). DLE measurements revealed only slight differences in the adsorption efficiency with the best values obtained by β- and γ-CD cryogels; this finding could be attributed to the planarity of these CDs which may have led to a less steric impedance when positioned among the polymeric chains.[54,56–58]

FLU showed a DLE of 52%, that is 13 mg g^{-1}, for HEMA and a value ranging from 46 to 78%, which corresponds to 11.5–19.5 mg g^{-1} for CD-HEMA cryogels (Fig. 2c), with an excellent adsorption amount in the case of Styr-β-CD reaching a DLE value of 78%. The capability of Styr-β-CD in adsorbing FLU can be derived from the volume of the β-CD cavity that is more
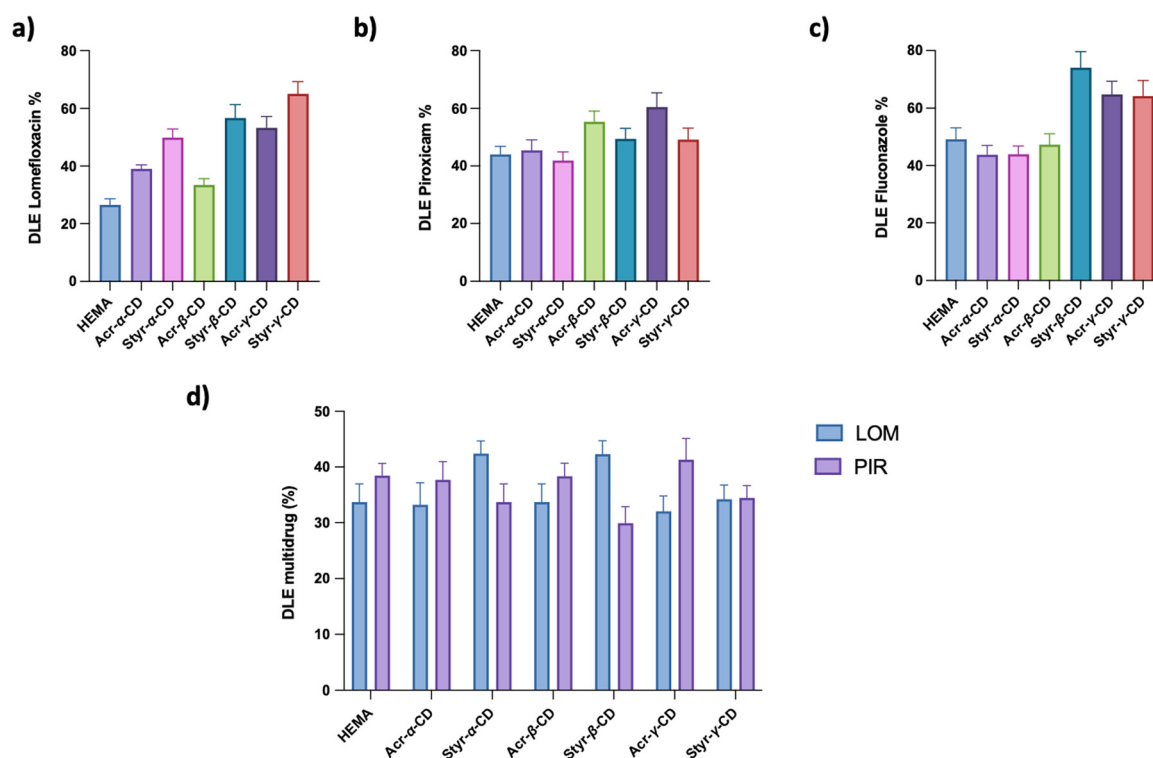

Fig. 2 Drug loading efficiency (DLE) after 24 h of adsorption of HEMA and CD-HEMA cryogels for (a) lomefloxacin (LOM), (b) piroxicam (PIR), (c) fluconazole (FLU), and (d) multi-drug loading system (LOM and PIR).

suitable for its spatial conformation. Interactions of styrenic moieties with the three aromatic rings of FLU may also play an important role.

PIR and LOM were contemporarily loaded in the same samples to design a wound healing system encompassing anti-inflammatory and antibacterial effects. The loading capacity for the multi-drug system was found to be 36% for LOM over HEMA, corresponding to 9 mg g^{-1}; the value ranged from 34 to 44% (8.5 to 11 mg g^{-1}) for CD-HEMA cryogels (Fig. 2d). Regarding PIR, the HEMA cryogel showed an uptake of 10 mg g^{-1} (40%), whereas values in the range 8–11 mg g^{-1} (32–44%) were shown by CD-HEMA cryogels. In such a case, the system's saturation may influence the DLE at the material-solution interface.

The HEMA cryogel, used as a reference, showed good adsorption of selected drugs. However, such behavior could be due to multiple nonspecific H-bonds rather than specific interactions with selected drugs.

SEM images were also recorded after the loading of drugs into the cryogels, which confirmed the success of drug loading, as shown in Fig. 3 (up). Comparing the images of the drug-loaded cryogels (Fig. 3b–e) with those of the untreated ones (Fig. 3a), it is possible to observe the lack of little spots corresponding to the agglomerates of drug molecules. Undoubtedly, part of the drug is inserted into CD cavities. However, as proved by the kinetics of release, it is evident that a portion of the loaded molecules would be deposited on the surface of the cryogel and between the polymeric chains. Moreover, considering the case of PIR, bearing a sulfur atom in its skeleton, the achievement of the drug loading was confirmed by energy dispersive X-ray analysis (EDX). Fig. 3 (down) shows the reported values of the EDX graph that show that the Acr-α-CD cryogel loaded with PIR was mainly composed of C, O, N, and S atoms.

Drug release

The release efficiencies of the drug-loaded cryogels in acidic buffer, pH 3, and saline buffer, pH 7.4 at 37 °C, were investigated. The experimental data are shown in Fig. 4. The release profiles of LOM, PIR, and FLU from HEMA and CD-HEMA cryogels were measured to study their response as a function of salinity and pH. The release of LOM in an acidic environment is particularly favored because almost 90% of the drug is released from both HEMA and CD-HEMA (Fig. 4a). However, the release of LOM from Acr-α-CD and Acr-β-CD was slightly inferior to that from Styr-α-CD and Styr-β-CD because LOM forms a hydrogen bond with the acrylic moieties. These bonds are undoubtedly stronger than π-stacking interactions that occur with the phenyl ring of the styrenyl derivatives. Acr-β-CD releases better than Acr-α-CD since its more extensive cavity favors the drug solvation and release.

For the same reason, the best results were obtained with Acr-CD. Indeed, the dimension of the cavity plays an important role since the release of the drug from a more extensive cavity is favored. Moreover, note that bigger cavities with more moieties could have successfully formed more drug-CD complexes, encapsulating a higher amount of drug ready to be released
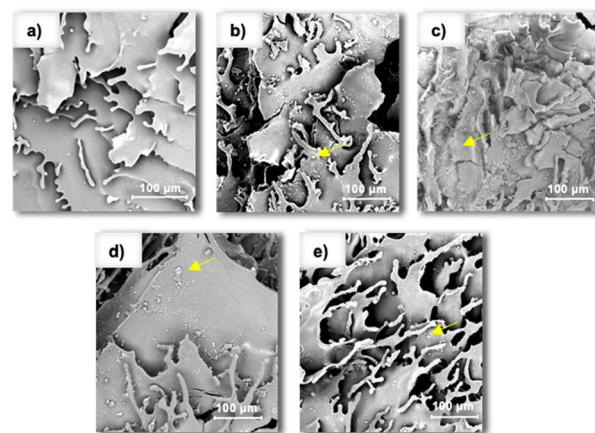
Element Symbol	Atomic Conc.	Weight Conc.
C	51.44	44.91
O	32.83	38.18
N	15.06	15.34
S	0.67	1.56

Fig. 3 (up) SEM images of (a) Acr-α-CD cryogels without the drug and with (b) LOM, (c) PIR, (d) FLU, and (e) multi-drug system. (down) EDX-derived atom percentage of the Acr-α-CD cryogel loaded with PIR.

in this step. In saline buffer, the LOM release ranged from 72% to 91%(Fig. 4b). Therefore, we can highlight that HEMA released only a minor part of the drug compared to Styr-γ-CD, while Acr-α-CD had a lower efficiency. Moreover, there were no relevant differences in the release between the other tested cryogels.

In the case of PIR, the release amount ranged from 23% to 71% in an acidic solution and from 25% to 60% in a saline buffer (Fig. 4c and d). In this case, it seems possible to note that acrylic moieties had a higher drug release efficiency than styrenic moieties in both acidic solution and saline buffer, which could be responsible for more stable interactions with PIR. According to the literature citing the PIR-β-CD complex, the release of PIR from β-CD was consistent under both acidic and saline conditions. Despite the successful loading of PIR into the synthesized cryogels, its release was found to be discouraged by the hydrophilic medium nature. Further studies will be required to establish whether the amount of released drug *in vivo* would be sufficient to show an anti-inflammatory effect. The release of PIR was higher for β-CD cryogels, possibly due to the presence of the molecules in the CD cavities rather than in the complex with the polymer matrix.

In the case of fluconazole, the release amount ranged between 46 and 92% in an acidic solution for HEMA and CD-HEMA cryogels, while in a saline buffer, it was between 53 and 79% (Fig. 4e and f). As reported for LOM, FLU showed a higher release amount from cryogels with styrenic moieties, with the maximum amount for Styr-γ-CD in an acidic solution and for Styr-α-CD in a saline buffer.

The multi-drug system cryogels of CD-HEMA showed higher release efficiency than HEMA in both acidic and saline buffers (Fig. 4g and h). In acidic solutions, Styr-α-CD and Styr-β-CD
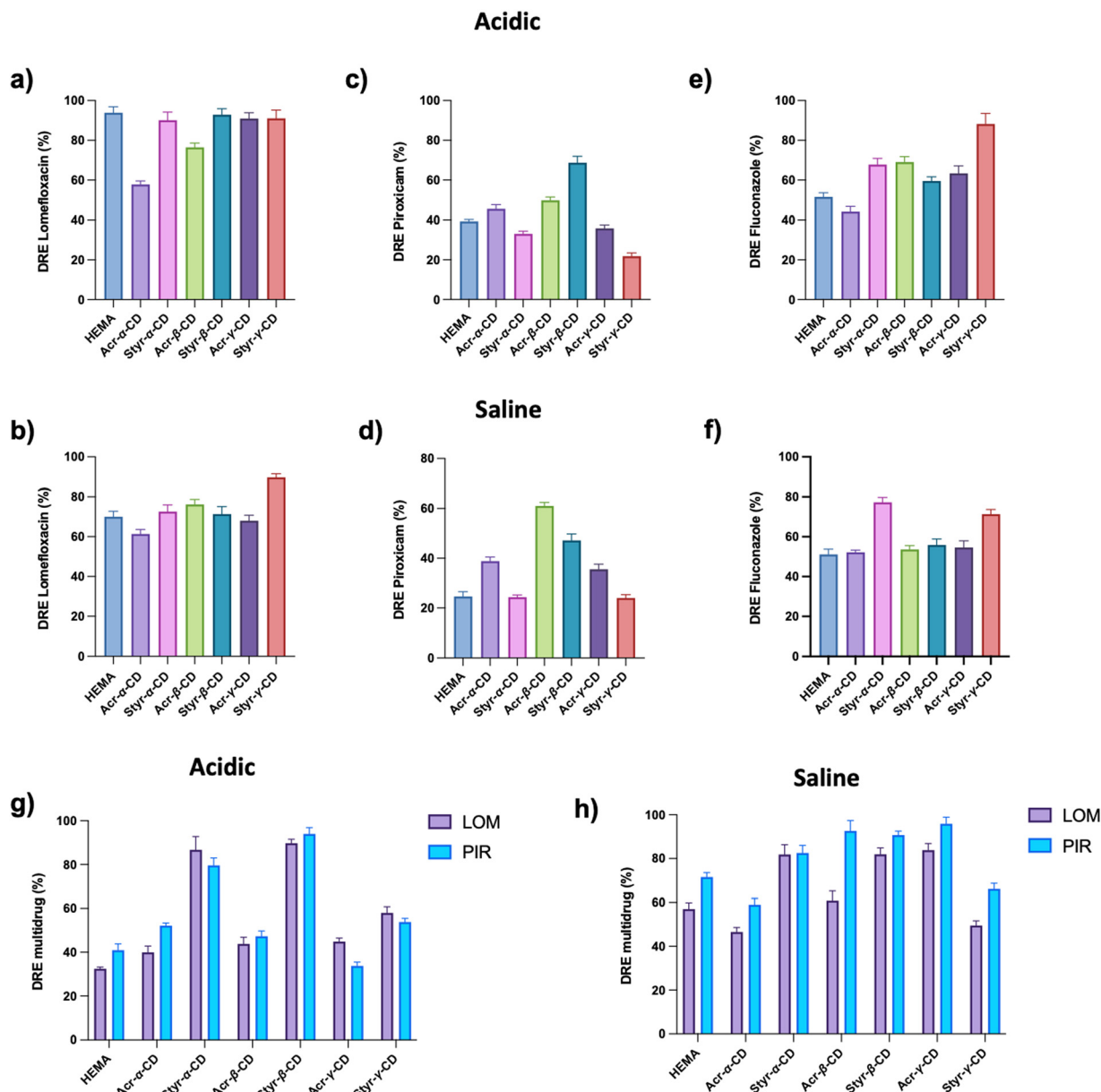
Fig. 4 Drug release efficiency (DRE) after 24 h in an acidic solution (pH = 3) and a saline buffer (pH = 7.4) of HEMA and CD-HEMA cryogels for (a and b) LOM, (c and d) PIR, and (e and f) FLU. DRE of HEMA and CD-HEMA cryogels for LOM and PIR in a multi-drug system in (g) acidic and (h) saline solutions.

displayed a higher drug release efficiency, while in a saline buffer, Styr-α-CD and Styr-β-CD, and Acr-γ-CD gave the best results. The results are not perfectly aligned with the single drug release; however, this may be due to multiple factors, such as release medium saturation, drug interactions in the matrix, and others. Overall, we can see good results for Styr-β-CD, confirmed from the literature as β-CD is often reported to form a complex with LOM and PIR.[55,59–61] Moreover, the styrenic moiety seemed suitable for loading and release as it can provide moderate π–π interactions.

Drug release kinetics

Looking at the release behavior (Fig. S23–S30, ESI†), we can see how a greater quantity of the drug is released in the first 5–8 hours. In fact, it was already reported in the literature that

proteins and drugs encapsulated in cryogels generally show an initial rapid burst release followed by a slower drug release.[62,63] Conversely, especially for the multi-drug release in the saline buffer (Fig. 5), it appears that styrene cryogels release the loaded drugs faster than acrylic cryogels reaching the equilibrium conditions after 5 hours, while acrylic cryogels can retain the loaded drug for a longer time and release it, continuously and in small amounts, within 24 h.

From the fitting analysis of the empirical data with the equations mentioned in the methods, two models showed the highest score (Tables S1–S5, ESI†). First, the Weibull model, with an R^2 value ranging from a minimum of 0.91 to a maximum of 0.999 and an average of 0.963, followed by the Korsmeyer–Peppas model, with an R^2 value ranging from a
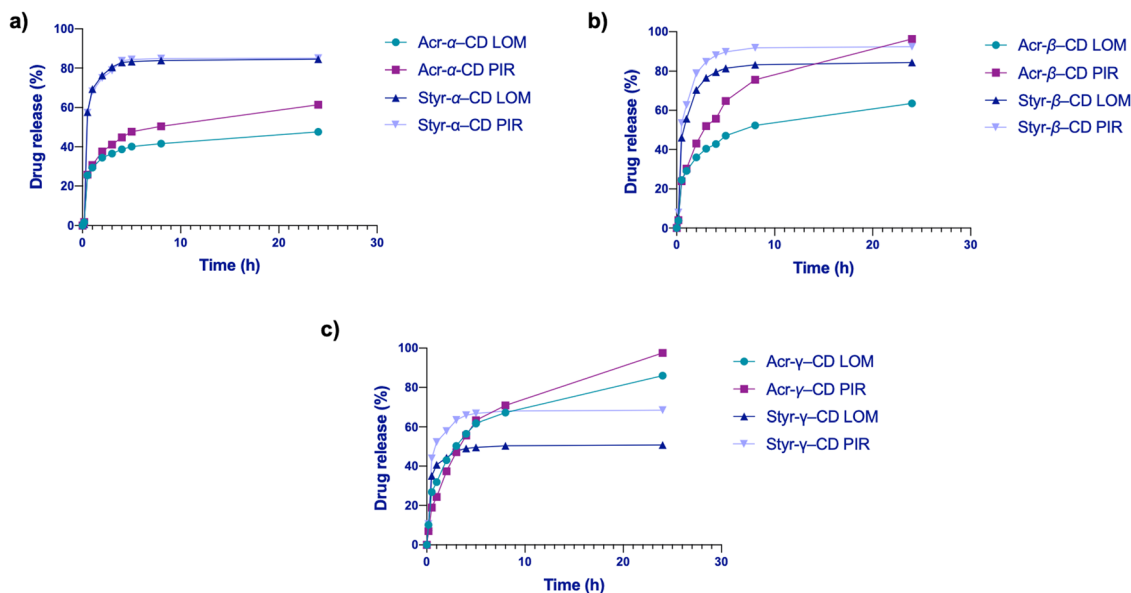
Fig. 5 Simultaneous drug release of LOM and PIR from (a) Acr- and Styr-α-CD, (b) Acr- and Styr-β-CD, and (c) Acr- and Styr-γ-CD cryogels in the saline buffer.

minimum of 0.898 to a maximum of 0.999 and an average of 0.952. The Higuchi model showed an average of R^2 of 0.925, significantly lower than the models mentioned above, demonstrating that the release was not dependent on system dissolution. The first-order and the zero-order models had lower R^2 values, indicating that their fitting was inappropriate (Tables S1–S5, ESI†). By way of examples, in Fig. 6 are reported all the fitting curves of the models previously described for Styr-β-CD, which is one of the most exciting samples. Both Weibull and Korsmeyer–Peppas models describe the release behavior from matrix systems, which is in accordance with our cryogel samples.

Moreover, both models seem to show a higher fitting for the release in a saline buffer. The Weibull model showed $b < 1$, indicating initial parabolic kinetics followed by an exponential decrease, while the release exponent in the Korsmeyer–Peppas model was mostly $n < 0.45$, indicating Fickian diffusion in most cases with some cases of $0.45 < n < 1.0$ anomalous transport, which comprises both diffusion and swelling.
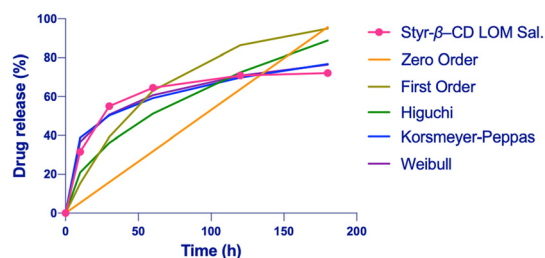
This suggests that the release behavior of cryogels is influenced by multiple factors.[45]

Considering the Weibull model, most likely, the release is a multi-step process: (1) fast release, the medium in contact with the surface of the cryogel permits the release of the drug adhered to the surface; (2) soon, the medium enters the matrix, causing swelling that favors the drug release from the macroporous polymeric network; and (3) medium enters the CD cavity thus displacing the drug. The burst effect of our system is well described by Weibull and Korsmeyer–Peppas models, reflecting the presence of a multi-step process for drug release of our cryogels as seen in analogous materials. This behavior may be beneficial in wound healing and burn skin applications, as the system will readily deliver LOM and PIR, preventing infections or inflammation.[64]

Cytocompatibility

The cytotoxicity of Acr-α-CD, Acr-β-CD, Acr-γ-CD, Styr-α-CD, Styr-β-CD, Styr-γ-CD, and HEMA cryogels was assessed using human dermal fibroblasts to confirm their biocompatibility and suitability as drug delivery systems. The outcomes are
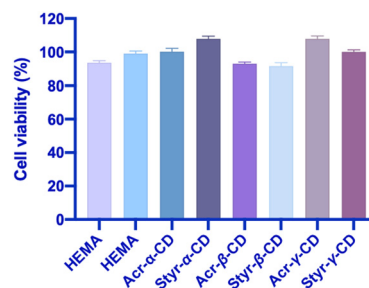

Fig. 6 Kinetic release fitting for Styr-β-CD with LOM in the saline buffer: zero-order model, $R^2 = 0.776$; first-order model, $R^2 = 0.928$; Higuchi model, $R^2 = 0.922$; Korsmeyer–Peppas model, $R^2 = 0.984$; and Weibull model, $R^2 = 0.99$.

Fig. 7 Cytocompatibility assay of CD-HEMA cryogels over the human fibroblastic cell line.

represented in Fig. 7. The viability of the treated cells incubated for 72 hours with HDFs was comparable to the vehicle-treated and untreated control cells. These results confirmed that the cryogels have acceptable biocompatibility and do not induce any cytotoxic effects over HDF cells.

Conclusions

Cryogels containing functionalized α, β, and γ-cyclodextrins have been prepared by exploiting new monomers specially designed for this purpose. Six different monomers were synthesized, Acr-α-CD, Acr-β-CD, Acr-γ-CD, Styr-α-CD, Styr-β-CD, and Styr-γ-CD, and used for the copolymerization in a cryo mode. To achieve a therapeutic effect, PIR, LOM, and FLU, in a single and dual formulation, were loaded into cryogels with DLE up to 78%, with the best results from γ-CD cryogels. At the same time, the release of selected pharmaceuticals was achieved by changing pH and salinity, reaching values up to 95%.

For all systems, a burst effect was observed in the first 3–5 hours, which was reasonable due to drug adsorption on material surfaces. This fast release is advantageous in the case of wound healing, especially in the treatment of skin wounds or burns. In addition, the drug release of the molecules embedded into the hydrophobic CD cavities within 24 hours ensures a treatment's continuity.

The cavity of the CDs plays a fundamental role in both loading and release processes, whereas the acrylic and styrenic moieties seem to form valuable interactions to stabilize the drug–CD complex while allowing the subsequent release. The release curves were fitted into different mathematical models, and it was found that the Weibull model was the best fit, with an R^2 value in the range of 0.91–0.999.

Finally, multi-drug systems were formulated with a dual objective of protecting the skin from bacterial infections while reducing the inflammatory process (Fig. S31, ESI†). This practical approach could be a game-changer in wound healing applications, representing a proof of concept that should be further investigated in the future.

Conflicts of interest

There are no conflicts to declare.

Acknowledgements

References

1 A. M. Vargason, A. C. Anselmo and S. Mitragotri, The evolution of commercial drug delivery technologies, *Nat. Biomed. Eng.*, 2021, **5**, 951–967.

2 M. J. Webber and R. Langer, Drug delivery by supramolecular design, *Chem. Soc. Rev.*, 2017, **46**, 6600–6620.

3 A. Tewabe, A. Abate, M. Tamrie, A. Seyfu and E. Abdela Siraj, Targeted Drug Delivery – From Magic Bullet to Nanomedicine: Principles, Challenges, and Future Perspectives, *J. Multidiscip. Healthc.*, 2021, **14**, 1711–1724.

4 L. Sercombe, T. Veerati, F. Moheimani, S. Y. Wu, A. K. Sood and S. Hua, Advances and Challenges of Liposome Assisted Drug Delivery, *Front. Pharmacol.*, 2015, **6**, 286.

5 P. Nakhaei, R. Margiana, D. O. Bokov, W. K. Abdelbasset, M. A. Jadidi Kouhbanani, R. S. Varma, F. Marofi, M. Jarahian and N. Beheshtkhoo, Liposomes: Structure, Biomedical Applications, and Stability Parameters With Emphasis on Cholesterol, *Front. Bioeng. Biotechnol.*, 2021, **9**, 705886.

6 S. Perumal, R. Atchudan and W. Lee, A Review of Polymeric Micelles and Their Applications, *Polymers*, 2022, **14**, 2510.

7 J. Li, Y. Wang, L. Zhang, Z. Xu, H. Dai and W. Wu, Nanocellulose/Gelatin Composite Cryogels for Controlled Drug Release, *ACS Sustain. Chem. Eng.*, 2019, **7**, 6381–6389.

8 V. Parmar, G. Patel and N. Y. Abu-Thabit, Responsive cyclodextrins as polymeric carriers for drug delivery applications, *Stimuli Responsive Polymeric Nanocarriers for Drug Delivery Applications*, Elsevier, 2018, **1**, 555–580.

9 Z. Liu, L. Ye, J. Xi, J. Wang and Z. Feng, Cyclodextrin polymers: Structure, synthesis, and use as drug carriers, *Prog. Polym. Sci.*, 2021, **118**, 101408.

10 M. L. Oyen, Mechanical characterisation of hydrogel materials, *Int. Mater. Rev.*, 2014, **59**, 44–59.

11 N. Kathuria, A. Tripathi, K. K. Kar and A. Kumar, Synthesis and characterization of elastic and macroporous chitosan–gelatin cryogels for tissue engineering, *Acta Biomater.*, 2009, **5**, 406–418.

12 P. Im and J. Kim, On-Demand Macroscale Delivery System Based on a Macroporous Cryogel with a High Drug Loading Capacity for Enhanced Cancer Therapy, *ACS Biomater. Sci. Eng.*, 2018, **4**, 3498–3505.

13 D. Çimen, M. A. Özbek, N. Bereli, B. Mattiasson and A. Denizli, Injectable Cryogels in Biomedicine, *Gels*, 2021, **7**, 38.

14 L. O. Jones, L. Williams, T. Boam, M. Kalmet, C. Oguike and F. L. Hatton, Cryogels: recent applications in 3D-bioprinting, injectable cryogels, drug delivery, and wound healing, *Beilstein J. Org. Chem.*, 2021, **17**, 2553–2569.

15 I. N. Savina, M. Zoughaib and A. A. Yergeshov, Design and assessment of biodegradable macroporous cryogels as advanced tissue engineering and drug carrying materials, *Gels*, 2021, **7**, 79.

16 S. Pacelli, L. Di Muzio, P. Paolicelli, V. Fortunati, S. Petralito, J. Trilli and M. A. Casadei, Dextran-polyethylene glycol cryogels as spongy scaffolds for drug delivery, *Int. J. Biol. Macromol.*, 2021, **166**, 1292–1300.

17 *Polymeric Cryogels*, ed. O. Okay, Springer International Publishing, Cham, 2014, vol. 263.

18 K. Yao, S. Shen, J. Yun, L. Wang, X. He and X. Yu, Preparation of polyacrylamide-based supermacroporous monolithic

cryogel beds under freezing-temperature variation conditions, *Chem. Eng. Sci.*, 2006, **61**, 6701–6708.

19 A. Memic, T. Colombani, L. J. Eggermont, M. Rezaeeyazdi, J. Steingold, Z. J. Rogers, K. J. Navare, H. S. Mohammed and S. A. Bencherif, Latest Advances in Cryogel Technology for Biomedical Applications, *Adv. Ther.*, 2019, **2**, 1800114.

20 I. N. Savina, G. C. Ingavle, A. B. Cundy and S. V. Mikhalovsky, A simple method for the production of large volume 3D macroporous hydrogels for advanced biotechnological, medical and environmental applications, *Sci. Rep.*, 2016, **6**, 21154.

21 *Supermacroporous Cryogels: Biomedical and Biotechnological Applications*, ed. A. Kumar, CRC Press, Boca Raton, 2016.

22 J. Kumari, A. A. Karande and A. Kumar, Combined Effect of Cryogel Matrix and Temperature-Reversible Soluble-Insoluble Polymer for the Development of in Vitro Human Liver Tissue, *ACS Appl. Mater. Interfaces*, 2016, **8**, 264–277.

23 J. K. Fink, *Reactive Polymers: Fundamentals and Applications: A Concise Guide to Industrial Polymers*, William Andrew, Amsterdam Netherlands, 3rd edn, 2017.

24 M. Zare, A. Bigham, M. Zare, H. Luo, E. Rezvani Ghomi and S. Ramakrishna, pHEMA: An Overview for Biomedical Applications, *Int. J. Mol. Sci.*, 2021, **22**, 6376.

25 E. Larrañeta, S. Stewart, M. Ervine, R. Al-Kasasbeh and R. F. Donnelly, Hydrogels for Hydrophobic Drug Delivery. Classification, Synthesis and Applications, *J. Funct. Biomater.*, 2018, **9**, 13.

26 R. Chang, Q. Zou, R. Xing and X. Yan, Peptide-Based Supramolecular Nanodrugs as a New Generation of Therapeutic Toolboxes against Cancer, *Adv. Ther.*, 2019, **2**, 1900048.

27 J. Liu, Y. Lan, Z. Yu, C. S. Y. Tan, R. M. Parker, C. Abell and O. A. Scherman, Cucurbit[n]uril-Based Microcapsules Self-Assembled within Microfluidic Droplets: A Versatile Approach for Supramolecular Architectures and Materials, *Acc. Chem. Res.*, 2017, **50**, 208–217.

28 M. M. Naseer, M. Ahmed and S. Hameed, Functionalized calix[4]arenes as potential therapeutic agents, *Chem. Biol. Drug Des.*, 2017, **89**, 243–256.

29 B. Qin, Z. Yin, X. Tang, S. Zhang, Y. Wu, J.-F. Xu and X. Zhang, Supramolecular polymer chemistry: From structural control to functional assembly, *Prog. Polym. Sci.*, 2020, **100**, 101167.

30 L. Peng, S. Liu, A. Feng and J. Yuan, Polymeric Nanocarriers Based on Cyclodextrins for Drug Delivery: Host–Guest Interaction as Stimuli Responsive Linker, *Mol. Pharm.*, 2017, **14**, 2475–2486.

31 M. A. Przybyla, G. Yilmaz and C. R. Becer, Natural cyclodextrins and their derivatives for polymer synthesis, *Polym. Chem.*, 2020, **11**, 7582–7602.

32 S. M. N. Simões, A. Rey-Rico, A. Concheiro and C. Alvarez-Lorenzo, Supramolecular cyclodextrin-based drug nanocarriers, *Chem. Commun.*, 2015, **51**, 6275–6289.

33 K. Uekama, Design and evaluation of cyclodextrin-based drug formulation, *Chem. Pharm. Bull.*, 2004, **52**, 900–915.

34 J. Ahmed, M. Gultekinoglu and M. Edirisinghe, Bacterial cellulose micro-nano fibres for wound healing applications, *Biotechnol. Adv.*, 2020, **41**, 107549.

35 T. Takei, S. Danjo, S. Sakoguchi, S. Tanaka, T. Yoshinaga, H. Nishimata and M. Yoshida, Autoclavable physically-crosslinked chitosan cryogel as a wound dressing, *J. Biosci. Bioeng.*, 2018, **125**, 490–495.

36 A. Górska, A. Krupa, D. Majda, P. Kulinowski, M. Kurek, W. P. Węglarz and R. Jachowicz, Poly(Vinyl Alcohol) Cryogel Membranes Loaded with Resveratrol as Potential Active Wound Dressings, *AAPS PharmSciTech*, 2021, **22**, 109.

37 A. Farooq, M. Yar, A. S. Khan, L. Shahzadi, S. A. Siddiqi, N. Mahmood, A. Rauf, Z.-A. Qureshi, F. Manzoor, A. A. Chaudhry and I. ur Rehman, Synthesis of piroxicam loaded novel electrospun biodegradable nanocomposite scaffolds for periodontal regeneration, *Mater. Sci. Eng., C*, 2015, **56**, 104–113.

38 A. Rescifina, C. Zagni, P. G. Mineo, S. V. Giofrè, U. Chiacchio, S. Tommasone, C. Talotta, C. Gaeta and P. Neri, DNA recognition with polycyclic-aromatic-hydrocarbon-presenting calixarene conjugates, *Eur. J. Org. Chem.*, 2014, 7605–7613.

39 C. Zagni, S. Dattilo, T. Mecca, C. Gugliuzzo, A. A. Scamporrino, V. Privitera, R. Puglisi and S. Carola Carroccio, Single and dual polymeric sponges for emerging pollutants removal, *Eur. Polym. J.*, 2022, **179**, 111556.

40 H. T. Hoang, T. T. Vu, V. Karthika, S.-H. Jo, Y.-J. Jo, J.-W. Seo, C.-W. Oh, S.-H. Park and K. T. Lim, Dual cross-linked chitosan/alginate hydrogels prepared by Nb-Tz 'click' reaction for pH responsive drug delivery, *Carbohydr. Polym.*, 2022, **288**, 119389.

41 M. L. Bruschi, *Strategies to modify the drug release from pharmaceutical systems*, Woodhead Publishing, 2015.

42 J. Siepmann and F. Siepmann, Mathematical modeling of drug dissolution, *Int. J. Pharm.*, 2013, **453**, 12–24.

43 S. Khan and N. M. Ranjha, Effect of degree of cross-linking on swelling and on drug release of low viscous chitosan/poly(vinyl alcohol) hydrogels, *Polym. Bull.*, 2014, **71**, 2133–2158.

44 R. W. Korsmeyer, R. Gurny, E. Doelker, P. Buri and N. A. Peppas, Mechanisms of solute release from porous hydrophilic polymers, *Int. J. Pharm.*, 1983, **15**, 25–35.

45 N. A. Peppas, Analysis of Fickian and non-Fickian drug release from polymers, *Pharm. Acta Helv.*, 1985, **60**, 110–111.

46 T. Higuchi, Mechanism of sustained-action medication. Theoretical analysis of rate of release of solid drugs dispersed in solid matrices, *J. Pharm. Sci.*, 1963, **52**, 1145–1149.

47 W. Weibull and A. Statistical, Distribution Function of Wide Applicability, *J. Appl. Mech.*, 1951, **18**, 293–297.

48 A. R. Khan, P. Forgo, K. J. Stine and V. T. D'Souza, Methods for Selective Modifications of Cyclodextrins, *Chem. Rev.*, 1998, **98**, 1977–1996.

49 Y. Bai, J. Wang, M. Bashari, X. Hu, T. Feng, X. Xu, Z. Jin and Y. Tian, A thermogravimetric analysis (TGA) method developed for estimating the stoichiometric ratio of solid-state α-cyclodextrin-based inclusion complexes, *Thermochim. Acta*, 2012, **541**, 62–69.

50 S. Pereva, V. Nikolova, S. Angelova, T. Spassov and T. Dudev, Water inside β-cyclodextrin cavity: amount, stability and

mechanism of binding, *Beilstein J. Org. Chem.*, 2019, **15**, 1592–1600.

51 F. Trotta, M. Zanetti and G. Camino, Thermal degradation of cyclodextrins, *Polym. Degrad. Stab.*, 2000, **69**, 373–379.

52 V. Chopra, J. Thomas, A. Sharma, V. Panwar, S. Kaushik and D. Ghosh, A bioinspired, ice-templated multifunctional 3D cryogel composite crosslinked through in situ reduction of GO displayed improved mechanical, osteogenic and antimicrobial properties, *Mater. Sci. Eng., C*, 2021, **119**, 111584.

53 B. Kost, M. Brzeziński, M. Socka, M. Baśko and T. Biela, Biocompatible Polymers Combined with Cyclodextrins: Fascinating Materials for Drug Delivery Applications, *Molecules*, 2020, **25**, 3404.

54 A. Rasheed, C. K. Ashok Kumar and V. V. N. S. S. Sravanthi, Cyclodextrins as Drug Carrier Molecule: A Review, *Sci. Pharm.*, 2008, **76**, 567–598.

55 V. Nanjwade, F. V. Manvi and B. Nanjwade, Formulation and Evaluation of Dispersible Tablets of Lomefloxacin HCl, *Int. J. Drug Dev. Res.*, 2013, **5**, 103–113.

56 O. E. Khoukhi, Z. E. Bahri, K. Diaf and M. Baitiche, Piroxicam/β-cyclodextrin complex included in cellulose derivatives-based matrix microspheres as new solid dispersion-controlled release formulations, *Chem. Pap.*, 2016, **70**, 828–839.

57 M. Sauceau, E. Rodier and J. Fages, Preparation of inclusion complex of piroxicam with cyclodextrin by using supercritical carbon dioxide, *J. Supercrit. Fluids*, 2008, **47**, 326–332.

58 G. M. Miranda, V. O. R. e Santos, J. R. Bessa, Y. C. F. Teles, S. C. M. A. Yahouédéhou, M. S. Goncalves and J. Ribeiro-Filho, Inclusion Complexes of Non-Steroidal Anti-Inflammatory Drugs with Cyclodextrins: A Systematic Review, *Biomolecules*, 2021, **11**, 361.

59 O. E. Khoukhi, Z. E. Bahri, K. Diaf and M. Baitiche, Piroxicam/β-cyclodextrin complex included in cellulose derivatives-based matrix microspheres as new solid dispersion-controlled release formulations, *Chem. Pap.*, 2016, **70**, 828–839.

60 M. Sauceau, E. Rodier and J. Fages, Preparation of inclusion complex of piroxicam with cyclodextrin by using supercritical carbon dioxide, *J. Supercrit. Fluids*, 2008, **47**, 326–332.

61 A. Rasheed, C. K. Ashok Kumar and V. V. N. S. S. Sravanthi, Cyclodextrins as Drug Carrier Molecule: A Review, *Sci. Pharm.*, 2008, **76**, 567–598.

62 S. T. Koshy, D. K. Y. Zhang, J. M. Grolman, A. G. Stafford and D. J. Mooney, Injectable nanocomposite cryogels for versatile protein drug delivery, *Acta Biomater.*, 2018, **65**, 36–43.

63 G. Pandey, N. Mittapelly, A. Pant, S. Sharma, P. Singh, V. T. Banala, R. Trivedi, P. K. Shukla and P. R. Mishra, Dual functioning microspheres embedded crosslinked gelatin cryogels for therapeutic intervention in osteomyelitis and associated bone loss, *Eur. J. Pharm. Sci.*, 2016, **91**, 105–113.

64 D. Momekova, Y. Danov, G. Momekov, E. Ivanov and P. Petrov, Polysaccharide Cryogels Containing β-Cyclodextrin for the Delivery of Cannabidiol, *Pharmaceutics*, 2021, **13**, 1774.